



HAL
open science

On the magnetization of gamma-ray burst blast waves

Martin Lemoine, Zhuo Li, Xiang-Yu Wang

► **To cite this version:**

Martin Lemoine, Zhuo Li, Xiang-Yu Wang. On the magnetization of gamma-ray burst blast waves. *Monthly Notices of the Royal Astronomical Society*, 2013, 435, pp.3009-3016. 10.1093/mnras/stt1494 . hal-03645448

HAL Id: hal-03645448

<https://hal.science/hal-03645448>

Submitted on 24 May 2022

HAL is a multi-disciplinary open access archive for the deposit and dissemination of scientific research documents, whether they are published or not. The documents may come from teaching and research institutions in France or abroad, or from public or private research centers.

L'archive ouverte pluridisciplinaire **HAL**, est destinée au dépôt et à la diffusion de documents scientifiques de niveau recherche, publiés ou non, émanant des établissements d'enseignement et de recherche français ou étrangers, des laboratoires publics ou privés.

On the magnetization of gamma-ray burst blast waves

Martin Lemoine,^{1★} Zhuo Li^{2,3★} and Xiang-Yu Wang^{4,5★}

¹*Institut d'Astrophysique de Paris, CNRS, UPMC, 98 bis boulevard Arago, F-75014 Paris, France*

²*Department of Astronomy/Kavli Institute for Astronomy and Astrophysics, Peking University, Beijing 100871, China*

³*Key Laboratory for the Structure and Evolution of Celestial Objects, Chinese Academy of Sciences, Kunming 650011, China*

⁴*School of Astronomy and Space Science, Nanjing University, Nanjing 210093, China*

⁵*Key laboratory of Modern Astronomy and Astrophysics (Nanjing University), Ministry of Education, Nanjing 210093, China*

Accepted 2013 August 7. Received 2013 July 18; in original form 2013 May 22

ABSTRACT

The origin of magnetic fields that permeate the blast waves of gamma-ray bursts (GRBs) is a long-standing problem. The present paper argues that in four GRBs revealing extended emission at >100 MeV, with follow-up in the radio, optical and X-ray domains at later times, this magnetization can be described as the partial decay of the micro-turbulence that is generated in the shock precursor. Assuming that the bulk of the extended emission >100 MeV can be interpreted as synchrotron emission of shock-accelerated electrons, we model the multi-wavelength light curves of GRB 090902B, GRB 090323, GRB 090328 and GRB 110731A, using a simplified then a full synchrotron calculation with power-law-decaying micro-turbulence $\epsilon_B \propto t^{\alpha_t}$ (t denotes the time since injection through the shock, in the comoving blast frame). We find that these models point to a consistent value of the decay exponent $-0.5 \lesssim \alpha_t \lesssim -0.4$.

Key words: acceleration of particles – shock waves – gamma-ray burst: general.

1 INTRODUCTION

In principle, the multi-wavelength light curves of gamma-ray bursts (GRBs) in the afterglow phase open a remarkable window on the physics of relativistic, weakly magnetized collisionless shock waves: these light curves are indeed thought to result from the synchrotron process of electrons accelerated at the external shock wave, so that their modelling leads to two microphysical parameters of importance: the fraction of shock dissipated energy stored in the suprathermal electron population, ϵ_e , and in the self-generated electromagnetic turbulence, ϵ_B .

From a theoretical point of view, one expects $\epsilon_B \sim 0.1$ at the shock front (and $\epsilon_e \sim 0.1$): the shock wave forms when a magnetic barrier on the ion skin depth scale $\sim c/\omega_{pi}$ builds up through small-scale electromagnetic instabilities, up to the level at which it can deflect by an angle of the order of unity the incoming particles, which carry Lorentz factor γ_{sh} in the shock front frame; this demands $\epsilon_B \sim 1/4$. This picture has been validated by high performance particle-in-cell (PIC) simulations (e.g. Spitkovsky 2008; Martins et al. 2009; Haugbølle 2011; Sironi & Spitkovsky 2011, 2013), and supported by theoretical arguments (e.g. Medvedev & Loeb 1999). However, on such small plasma scales, the micro-turbulence should decay rapidly behind the shock (e.g. Gruzinov & Waxman 1999), whereas early afterglow models of GRBs have pointed to finite, substantial values of ϵ_B on the (comoving) scale of the blast $\sim ct_{dyn}$ [with

$t_{dyn} \sim r/(\gamma_b c)$ the dynamical time-scale, γ_b the blast Lorentz factor], many orders of magnitude larger than the skin depth scale (e.g. Piran 2004, and references therein):¹ $t_{dyn}\omega_{pi} \sim 2 \times 10^7 E_{54}^{1/8} n_0^{3/8} t_2^{5/8}$. Nevertheless, the decay of Weibel turbulence has been observed in dedicated numerical experiments (Chang, Spitkovsky & Arons 2008; Keshet et al. 2009; Medvedev et al. 2011), although admittedly, such simulations can probe only a small fraction of a GRB dynamical time-scale.

The detection of extended high energy emission >100 MeV by the *Fermi*-LAT instrument in several GRBs has brought in new constraints in this picture. Most notably, the synchrotron model of this emission has pointed to values of ϵ_B much smaller than unity in an adiabatic scenario (Kumar & Barniol-Duran 2009, 2010; Barniol-Duran & Kumar 2011; He et al. 2011; Liu & Wang 2011). Kumar & Barniol-Duran (2009) have noted that the magnetic field in which the electrons radiate corresponds to a strength $\sim 10 \mu\text{G}$ in the upstream frame, before shock compression; they therefore interpret this magnetic field as the simple shock compression of the interstellar field. However, the fact that the inferred ϵ_B lies a few orders of magnitude above the interstellar magnetization level $\sim 10^{-9}$ rather suggests that the electrons radiate in a partially decayed micro-turbulence (Lemoine 2013); theoretically, such a picture could reconcile the results of PIC simulations with the observational determinations of ϵ_B .

* E-mail: lemoine@iap.fr (ML); zhou.li@pku.edu.cn (ZL); xywang@nju.edu.cn (XYW)

¹ We use the standard notation $Q_x \equiv Q/10^x$ in CGS units, unless otherwise noted.

In the present work, we push forward this idea and put it to the test by considering the multi-wavelength light curves of four GRBs observed in radio, optical, X-ray and GeV in the framework of a decaying micro-turbulence afterglow scenario. We show that these four bursts point to a consistent value of the decay index $-0.5 \lesssim \alpha_t \lesssim -0.4$, if one assumes that $\epsilon_B \propto t^{\alpha_t}$, with t the time since injection of the plasma through the shock, as measured in the comoving blast frame, and $\epsilon_B \sim 0.01$ at $t = 100\omega_{\text{pi}}^{-1}$, as observed in PIC simulations. To do so, we first present a simplified model of this afterglow (Section 2), with two radiating zones, in each of which one can use the standard afterglow model (e.g. Sari, Piran & Narayan 1998); then we provide a detailed treatment of the power-law decay of the micro-turbulence (Section 2.3), improving on Lemoine (2013). We confront our findings to previous results in Section 3.

2 AFTERGLOW MODEL

2.1 General considerations

The calculation of the synchrotron spectrum of a relativistic blast wave with decaying micro-turbulence can be approximated (and much simplified) by noting that photons in different frequency bands have been emitted by electrons of different Lorentz factors, which cool at different times since their injection, hence in regions of different magnetic field strengths. In this approximate treatment, one can therefore use the standard homogeneous afterglow model for each frequency band, allowing for a possibly different ϵ_B in each band. When compared to the detailed calculations with decaying micro-turbulence, one finds that the above provides a reasonable approximation, provided the decay index $\alpha_t \gtrsim -1$. We make this approximation in the present work and justify it a posteriori.

According to the above picture, one should take a similar ϵ_{B-} for all frequencies $\nu < \nu_c$ that correspond to Lorentz factors $\gamma < \gamma_c$ such that the cooling time-scale exceeds the dynamical time-scale, $t_{\text{cool}}(\gamma) \gtrsim t_{\text{dyn}}$. Such particles indeed radiate most of their synchrotron energy in the same region, at the back of the blast. For GRB afterglows with extended > 100 MeV emission, in which we are interested here, this concerns the radio and optical range, and possibly the X-ray range at late times. For those frequencies, one can therefore use the standard homogeneous approximation of slowly cooling particles for the calculation of F_ν .

At the other extreme, GeV photons are likely produced in a region of strong ϵ_B , due to the short cooling time-scale of the emitting parent electrons. The large Lorentz factors also generally imply that inverse Compton losses are negligible in this frequency range due to Klein–Nishina (KN) suppression, although this should be verified on a case-to-case basis. Given these assumptions, the expected flux depends on the ejecta kinetic energy E and ϵ_e , but very little on the other parameters, ϵ_B in particular. Indeed, the energy radiated in the GeV range corresponds to $\sim (\gamma_8/\gamma_{\text{min}})^2 \sim s$ times the blast energy stored in the electron distribution $\propto \epsilon_e E$, where γ_8 denotes the minimum Lorentz factor of electrons radiating at > 100 MeV. It is easy to see that $\gamma_8/\gamma_{\text{min}} \propto \epsilon_B^{-1/4}$, so that the residual dependence of $F_\nu (> 100 \text{ MeV})$ on ϵ_B is quite small. As inverse Compton losses can be neglected at those energies, the flux does not depend either on the external density n . As already noted in Kumar & Barniol-Duran (2009), the flux density $F_\nu (> 100 \text{ MeV})$ provides a unique constraint on the model parameters, all the more so in the present case of decaying micro-turbulence.

The application of the above simple algorithm allows us to evaluate the parameters of the afterglow in the framework of the standard model. One outcome of this analysis is the measurement of ϵ_{B-} , which represents the value of ϵ_B at the back of the blast, through the modelling of the radio, optical and X-ray flux. Since the dynamical time-scale is determined by the standard parameters of the blast, one can constrain directly the exponent of power-law decay α_t :

$$\alpha_t = \frac{\log[\epsilon_{B-}/\epsilon_{B+}]}{\log[t_{\text{dyn}}/\tau_{\delta B}]}, \quad (1)$$

up to logarithmic corrections dependent on $\tau_{\delta B} \sim 100\omega_{\text{pi}}^{-1}$, the time-scale beyond which turbulence starts to decay and $\epsilon_{B+} \sim 0.01$, the value of the micro-turbulence close to the shock front, both of which are constrained by PIC simulations.

Care must be taken in the course of this exercise, because for low ϵ_{B-} , the Compton parameter at the cooling frequency $Y_c \gg 1$, and KN suppression of the inverse Compton process may be efficient in the X-ray range at late times. The magnitude of KN suppression at frequency ν can be quantified through the following equation:

$$\Upsilon_{\text{KN}}(\nu) \equiv \frac{h\nu_c(1+z)\gamma(\nu)}{\gamma_b m_e c^2} \simeq 50 E_{54}^{1/4} t_5^{1.36} A_{35}^{-2.10} \epsilon_{B-, -5}^{-0.80} \epsilon_{e, -1}^{-1.16} v_{17.38}^{1/2}, \quad (2)$$

where $\gamma(\nu)$ denotes the Lorentz factor of electrons whose (observer frame) synchrotron peak frequency equals ν . For the numerical values, we have assumed a wind profile of external density $n = 10^{35} A_{35} r^{-2} \text{ cm}^{-3}$, an electron spectral index $p = 2.2$, $\nu > \nu_c$ with Y_c given by Sari & Esin (2001) in the slow cooling regime and $z = 1$. $\Upsilon_{\text{KN}} > 1$ at X-ray frequencies means that KN suppression of the inverse Compton cooling is efficient and cannot be ignored.

The optical and radio data of the following light curves always lie below ν_c , in which case the Compton parameter does not depend on the electron Lorentz factor, $Y(\gamma) = Y_c$, the Compton parameter at γ_c (or equivalently, ν_c). In contrast, at GeV energies KN suppression is so efficient that the Compton parameter $Y_{>100 \text{ MeV}} \ll 1$ (e.g. Wang et al. 2010; Liu & Wang 2011). Therefore, inverse Compton losses with substantial KN suppression, which modify the synchrotron spectrum (e.g. Nakar, Ando & Sari 2009; Wang et al. 2010), concern only the X-ray domain at late times.

We therefore proceed as follows. We first search a solution assuming $\Upsilon_{\text{KN}} < 1$ in the X-ray range, with possibly large Y_c . We then compute Υ_{KN} , and if $\Upsilon_{\text{KN}} > 1$, we look for another solution in which we take into account the effect of KN suppression in the X-ray domain, following Li & Waxman (2006), Nakar et al. (2009) and Wang et al. (2010). In particular, we solve the following equations for the cooling Lorentz factor γ_c and Compton parameter Y_c at the cooling frequency:

$$(1 + Y_c)\gamma_c = \gamma_{c, \text{syn}}, \quad Y_c(1 + Y_c) = \frac{\epsilon_e}{\epsilon_{B-}} \left(\frac{\gamma_c}{\gamma_{\text{min}}} \right)^{2-p} \left[\min \left(1, \frac{\hat{\gamma}_c}{\gamma_c} \right) \right]^{(3-p)/2}, \quad (3)$$

with (see Nakar et al. 2009; Wang et al. 2010)

$$\gamma_{c, \text{syn}} \equiv \gamma_c|_{Y_c \rightarrow 0}, \quad \hat{\gamma}_c \equiv \frac{\gamma_b m_e c^2}{h\nu_c(1+z)}. \quad (4)$$

We neglect more extreme cases in which the electron interacts with low-frequency bands of the synchrotron spectrum, below ν_{min} . We then consider a synchrotron spectrum in the slow cooling phase (generic in the cases that we study) $F_\nu \propto t_{\text{obs}}^{-\alpha} \nu^{-\beta}$ with $\beta = 3(p-1)/4$ above ν_c instead of $\beta = p/2$ when $\Upsilon_{\text{KN}} < 1$. We

then verify a posteriori that the Compton parameter in the X-ray range $Y_X > 1$, if the X-ray range is fitted with this modified spectrum. In the GeV range, we always find $Y_{>100\text{MeV}} \ll 1$ due to KN suppression; therefore, we keep $\beta = p/2$ in that range. In Section 2.3, we incorporate the influence of decaying micro-turbulence, which modifies further the time and frequency dependencies of the synchrotron afterglow flux.

Finally, let us stress that while we assume that the bulk of the emission at energy >100 MeV originates from synchrotron radiation, we do not exclude that a fraction of the highest energy photons are actually produced by inverse Compton processes. In (homogeneous) small-scale turbulence, the high energy electrons suffer only small angular deflections as they cross a coherence length of the turbulence, so that their residence time (hence the acceleration time) becomes substantially larger than the gyrotime, which sets the residence time in a large-scale field (although advection impedes acceleration in large-scale turbulence; see Lemoine, Pelletier & Revenu 2006). Hence, in small-scale turbulence peaked on a wavelength $\lambda = 10 c/\omega_{\text{pi}}$ with $\epsilon_{B+} = 0.01$, the maximum synchrotron photon energy falls to 1–3 GeV at an observed time of 100 s for generic GRB afterglow parameters, see e.g. Kirk & Reville (2010), Bykov et al. (2012), Plotnikov, Pelletier & Lemoine (2013), Lemoine (2013) and Wang, Liu & Lemoine (2013), compared to a few tens of GeV for the ideal case of Bohm acceleration on a gyrotime, e.g. Lyutikov (2010). In a decaying micro-turbulence, the maximum photon energy does not depart much from the value for homogeneous small-scale turbulence with $\epsilon_{B+} = 0.01$, see Lemoine (2013), because the highest energy electrons cool on a relatively short time-scale, in regions of strong ϵ_B and at the same time interact with modes of wavelength larger than λ . For instance, a value of $\simeq 2$ GeV is derived at 100 s assuming that the minimum scale of the turbulence $\lambda = 10 c/\omega_{\text{pi}}$ for a decay index $\alpha_t = -0.5$ and a damping time of the turbulent modes $\tau \propto \lambda^2$. In this context, one should thus expect that photons of energy $\gtrsim 10$ GeV do not originate from synchrotron radiation, but from inverse Compton interactions, see Wang et al. (2013). However, the bulk of the emission >100 MeV can be produced by synchrotron radiation and we make this assumption in the present work. The energy interval 100 MeV–10 GeV indeed represents the bulk of the emission for the GRBs seen with extended emission, because their photon indices are $\simeq -2$, see Ackermann et al. (2013b). Of course, we verify a posteriori that the predicted synchrotron self-Compton (SSC) contribution does not exceed the synchrotron flux at energies >100 MeV.

2.2 Application to four *Fermi*-LAT GRBs

We now discuss the application of this exercise to four GRBs observed in the radio, optical, X-ray and GeV range: GRB 090902B, GRB 090323, GRB 090328 and GRB 110731A. We select them because four observational constraints (corresponding to the four frequency bands) are required to determine unambiguously the four parameters: ϵ_e , ϵ_{B-} , E and n . These four bursts have been discussed in the literature: the first three by Cenko et al. (2011) and the last one by Ackermann et al. (2013a). We will compare our results to these studies in Section 3.

2.2.1 GRB 090902B

We assume in the following $p = 2.3$, as suggested by the previous analyses of Cenko et al. (2011), Kumar & Barniol-Duran (2010),

Barniol-Duran & Kumar (2011) and Liu & Wang (2011), and $k = 0$ (constant density profile). The flux density at 100 MeV reads

$$F_\nu \simeq 6 \times 10^{-9} \text{ Jy } E_{54}^{1.05} \epsilon_{B+,-2}^{0.05} \epsilon_{e,-1}^{1.2} t_2^{-1.15}, \quad (5)$$

so that its measured value $\simeq 0.22 \mu\text{Jy}$ at a time $t_{\text{obs}} = 50$ s leads to

$$E_{54} \simeq 11.1 \epsilon_{e,-1}^{-1.21}. \quad (6)$$

We have discarded the dependence on the Compton parameter $Y_{>100\text{MeV}} \ll 1$ and on ϵ_{B+} , since we assume that the value of ϵ_{B+} that would enter this equation is close to 0.01, and its exponent is small.

For the optical range in the R band at ν_{opt} , we assume $\nu_{\text{min}} < \nu_{\text{opt}} < \nu_c$ at $t_{\text{obs}} = 65\,000$ s, with flux density 1.8×10^{-5} Jy. Therefore, the optical flux

$$F_\nu \simeq 0.088 \text{ Jy } E_{54}^{1.3} n_{-2}^{0.5} \epsilon_{B-,-2}^{0.8} \epsilon_{e,-1}^{1.2} t_2^{-0.9} \quad (7)$$

leads to the constraint, once equation (6) has been taken into account:

$$\epsilon_{B-,-2} \simeq 4.1 \times 10^{-5} \epsilon_{e,-1}^{0.37} n_0^{-0.61}. \quad (8)$$

Quite interestingly, these two GeV and optical determinations lead by themselves to very low values of ϵ_{B-} , provided that $\epsilon_{e,-1}$ and n_0 do not differ strongly from unity. The radio flux at $\nu_{\text{rad}} = 8.5$ GHz lies in the range of $\nu_{\text{rad}} < \nu_{\text{min}} < \nu_c$ at $t_{\text{obs}} \sim 10^5$ s, so that

$$F_\nu \simeq 4.2 \times 10^{-5} \text{ Jy } E_{54}^{5/6} \epsilon_{B-,-2}^{1/3} n_{-2}^{1/2} t_2^{1/2} \epsilon_{e,-1}^{-2/3}, \quad (9)$$

to be matched to $F_\nu \sim 1.3 \times 10^{-4}$ Jy at 4.8×10^5 s; when combined with the above equations (6) and (8), this implies

$$n_0 \simeq 2.5 \times 10^{-6} \epsilon_{e,-1}^{5.21}. \quad (10)$$

The decay rate in the X-ray range at $t_{\text{obs}} > 10^5$ s suggests that $\nu_c < \nu$ (see Liu & Wang 2011), which therefore brings in complementary constraints relatively to the optical and radio domains. In principle, one should allow for a different ϵ_B parameter in the region in which X-rays are produced; here, we make however the approximation that this $\epsilon_B \sim \epsilon_{B-}$. In Section 2.3, we compute the afterglow allowing for the dependence of ϵ_B on location, thus correcting this approximation.

If one first neglects KN suppression in the X-ray range, one is led to a solution with $\epsilon_{e,-1} \sim 2.7$, but with $\Upsilon_{\text{KN}} \sim 350$ at times 5×10^5 s, so that one needs to include the KN suppression. Following the above algorithm, and using the X-ray flux measurement between 0.3 and 10 keV of $2.2 \times 10^{-13} \text{ erg cm}^{-2} \text{ s}^{-1}$ at 5.2×10^5 s, with $\nu_X > \nu_c$, one derives ϵ_e , hence the parameter set

$$\begin{aligned} \epsilon_e &\simeq 0.46, & E &\simeq 1.8 \times 10^{54} \text{ erg}, \\ \epsilon_{B-} &\simeq 1.5 \times 10^{-5}, & n &\simeq 7.0 \times 10^{-3} \text{ cm}^{-3}. \end{aligned} \quad (11)$$

We also note that $\nu_c \simeq 8.2 \times 10^{16}$ Hz at 5.2×10^5 s, $Y_c \sim 27$, just as $\nu_{\text{rad}} < \nu_{\text{min}}$ and $\nu_{\text{min}} < \nu_{\text{opt}} < \nu_c$ at the respective times; the solution is therefore consistent.

This light curve therefore indicates a low value for ϵ_{B-} , corresponding to a decay exponent

$$\alpha_t \simeq -0.44 \pm 0.10, \quad (12)$$

assuming $\epsilon_{B+} = 0.01$ at $t = 100 \omega_{\text{pi}}^{-1}$. We used the value of t_{dyn} at time 10^5 s, at which the predicted spectrum has been normalized to the optical and radio data. We derive the uncertainty on α_t by propagating conservative estimates of the uncertainties in the value of p , of k and the statistical errors of the data used for normalization. As p goes from 2.1 to 2.5, α_t changes from -0.36 to -0.48 . If $k = 2$

instead of 0, one finds $\alpha_t = -0.51$.² For this burst, scintillation in the radio range provides the largest source of uncertainty, leading to a conservative factor ~ 3 uncertainty on the flux, which in turn leads to an error $\simeq 0.03$ on α_t . In total, we estimate the uncertainty $\Delta\alpha_t \simeq 0.10$.

2.2.2 GRB 090323

We repeat the same exercise with GRB 090323, which has been observed at >100 MeV up to a few hundred seconds, and in the X-ray, optical and radio domains, short of a day onwards. In what follows, we use $p = 2.5$, slightly smaller than the value found by Cenko et al. (2011) in their best fit, and $k = 2$. The >100 MeV flux is normalized to $\phi(>100 \text{ MeV}) = 1.5 \times 10^{-5}$ photon $\text{cm}^{-2} \text{s}^{-1}$ at 350 s, leading to

$$E_{54} \simeq 27.7 \epsilon_{e,-1}^{-1.33}, \quad (13)$$

while the optical flux is normalized to 1.3×10^{-5} Jy at 1.6×10^5 s, assuming $\nu_{\min} < \nu_{\text{opt}} < \nu_c$, leading to

$$\epsilon_{B,-2} \simeq 2.1 \times 10^{-3} A_{35}^{-1.14} \epsilon_{e,-1}^{-0.38}, \quad (14)$$

once equation (13) has been taken into account; then normalization to the radio flux $2. \times 10^{-4}$ Jy at 4.3×10^5 s with $\nu_{\text{rad}} < \nu_{\min} < \nu_c$ leads to

$$A_{35} \simeq 0.98 \epsilon_{e,-1}^2. \quad (15)$$

Here as well, note that the radio, optical and GeV constraints lead to a very low value for ϵ_B , if one assumes a parameter ϵ_e close to the value inferred in PIC simulations, $\epsilon_{e,-1} \sim 1$. To account for the X-ray flux, $\simeq 10^{-13}$ erg $\text{cm}^{-2} \text{s}^{-1}$ at 2.5×10^5 s, it is here as well necessary to consider the influence of KN suppression, which eventually leads to

$$\epsilon_e \simeq 0.25, \quad E \simeq 8.1 \times 10^{54} \text{ erg},$$

$$\epsilon_{B-} \simeq 1.8 \times 10^{-6}, \quad A \simeq 6.1 \times 10^{35} \text{ cm}^{-1}. \quad (16)$$

This corresponds to a decay index

$$\alpha_t \simeq -0.54 \pm 0.09, \quad (17)$$

where the error accounts for a factor of 2 uncertainty on the GeV flux (leading to ± 0.06 on α_t), a factor of 2 uncertainty on the radio determination (leading to ± 0.03) and an uncertainty $\Delta p = \pm 0.2$ (leading to ± 0.04); finally, if $k = 0$ instead of $k = 2$, one finds $\alpha_t = -0.50$.

2.2.3 GRB 090328

The multi-wavelength light curve for this burst is rather similar to that of GRB 090323, and we proceed analogously. Using a >100 MeV flux of 2.9×10^{-6} photon $\text{cm}^{-2} \text{s}^{-1}$ at 1.1×10^3 s, we obtain

$$E_{54} \simeq 2.1 \epsilon_{e,-1}^{-1.33}, \quad (18)$$

² The multi-wavelength light curve with a wind profile $k = 2$ does not provide as good a fit to the data as that with $k = 0$; however, it leads to a relatively high external wind parameter at early times, $A \sim 10^{35} \text{ cm}^{-1}$, which in turn implies a significant inverse Compton contribution at >100 MeV. Such a contribution could potentially explain the origin of the highest energy photon at ~ 30 GeV, which is difficult to account for in a scenario with $k = 0$; see Wang et al. (2013).

while the optical flux is normalized to 3×10^{-5} Jy at 0.6×10^5 s (with $\nu_{\min} < \nu_{\text{opt}} < \nu_c$), leading to

$$\epsilon_{B,-2} \simeq 1.5 \times 10^{-3} A_{35}^{-1.14} \epsilon_{e,-1}^{-0.38}. \quad (19)$$

Normalization to the radio flux 6×10^{-4} Jy at 3×10^5 s ($\nu_{\text{rad}} < \nu_{\min} < \nu_c$) leads to

$$A_{35} \simeq 0.4 \epsilon_{e,-1}^2. \quad (20)$$

The X-ray flux is normalized to 2.7×10^{-12} erg $\text{cm}^{-2} \text{s}^{-1}$ at 0.63×10^5 s, in the KN regime, which leads to ϵ_e , hence

$$\epsilon_e \simeq 0.19, \quad E \simeq 0.88 \times 10^{54} \text{ erg},$$

$$\epsilon_{B-} \simeq 7.6 \times 10^{-6}, \quad A \simeq 1.5 \times 10^{35} \text{ cm}^{-1}. \quad (21)$$

This corresponds to a decay index

$$\alpha_t \simeq -0.46 \pm 0.11, \quad (22)$$

at time 10^5 s. The error accounts for a factor of 2 uncertainty on the GeV flux (leading to ± 0.06 on α_t), a factor of 2 uncertainty on the radio determination (leading to ± 0.02) and an uncertainty $\Delta p = \pm 0.2$ (leading to ± 0.08); finally, if $k = 0$ instead of $k = 2$, one finds $\alpha_t = -0.42$.

2.2.4 GRB 110731A

This burst presents the most comprehensive multi-wavelength follow-up of a LAT burst with extended emission at >100 MeV; X-ray and optical start short of 100 s, while >100 MeV emission is still ongoing. Unfortunately, there are no radio detections for this burst, only an upper limit of 5×10^{-5} Jy at 0.58×10^5 s (Zauderer et al. 2011). Nevertheless, one can obtain strong constraints on ϵ_B , by noting that the optical frequency $\nu_{\text{opt}} = 5.5 \times 10^{14}$ Hz must satisfy $\nu_{\text{opt}} > \nu_{\min}$ at $t_{\text{obs}} = 100$ s, because the optical decays as a power law with index $\alpha \simeq 1.37$; if the opposite inequality were to hold at this time, one would rather observe $\alpha = 0$ for slow cooling, or $\alpha = 1/4$ for fast cooling. We thus write $\nu_{\min} = C_\nu \nu_{\text{opt}}$ with $C_\nu > 1$ at 100 s, which imposes

$$\epsilon_{B,-2} \simeq 5.1 \times 10^{-4} C_\nu^{-2} E_{54}^{-1} \epsilon_{e,-1}^{-4}. \quad (23)$$

Here and in the following, we assume $p = 2.1$ and $k = 2$. Given that $C_\nu > 1$, this obviously restricts ϵ_B to very low values, if E and ϵ_e take close to standard values. We next normalize the predicted F_ν to the observed optical flux density $\simeq 3.5 \times 10^{-4}$ Jy at 1100 s, assuming $\nu_{\min} < \nu_{\text{opt}} < \nu_c$ (verified a posteriori), which leads to

$$A_{35} \simeq 1.5 C_\nu^{1.55} \epsilon_{e,-1}^2. \quad (24)$$

The above two conditions imply a radio flux which is a factor of $\simeq 4.1$ in excess of the observational upper bound; this remains reasonable given the amount of scintillation typically expected at this time, and seen in the other bursts. We then use the >100 MeV flux, $\phi(>100 \text{ MeV}) \simeq 8.4 \times 10^{-5}$ photon $\text{cm}^{-2} \text{s}^{-1}$ at 26 s, to derive

$$E_{54} \simeq 2.5 \epsilon_{e,-1}^{-1.07}, \quad (25)$$

and finally the X-ray flux, 2×10^{-9} erg $\text{cm}^{-2} \text{s}^{-1}$ at 100 s, assuming $\nu_c < \nu_X$. For this burst, KN suppression is not effective at such an early time and it can be neglected in the normalization; however, ν_c is eventually found to be close to 1 keV, which makes this solution only approximate. In Section 2.3, we derive a better fit by adjusting by hand the missing parameter $\epsilon_{e,-1}$ under the above constraints.

Modulo this small uncertainty, the X-ray flux leads to

$$\begin{aligned}\epsilon_e &\simeq 0.021 C_v^{-0.50}, & E &\simeq 13. \times 10^{54} C_v^{0.54} \text{ erg}, \\ \epsilon_{B-} &\simeq 1.9 \times 10^{-4} C_v^{-0.53}, & A &\simeq 0.068 \times 10^{35} C_v^{0.54} \text{ cm}^{-1}.\end{aligned}\quad (26)$$

This implies a decay index

$$\alpha_t \simeq -0.35 \frac{1 + 0.51 \ln C_v}{1 + 0.10 \ln C_v}, \quad (27)$$

at $t_{\text{obs}} = 1100$ s. Assuming $C_v = 1$, we estimate a conservative uncertainty on α_t to be $\Delta\alpha_t \simeq \pm 0.2$ given that a factor of 2 uncertainty on the GeV flux leads to an error ± 0.10 , $p = 2.01$ leads to $\alpha_t = -0.14$ while $p = 2.3$ leads to $\alpha_t = -0.53$. Note that the light curves leave very little ambiguity on the density profile (Ackermann et al. 2013a); therefore, we do not consider $k = 0$.

2.3 Multi-wavelength light curves in a decaying turbulence

We now include the effect of decaying micro-turbulence. The changing magnetic field modifies the spectral shape of electrons with $\gamma > \gamma_c$, as well as the characteristic frequencies and their evolution in time (Lemoine 2013). With respect to the previous two-zone slow-cooling model, most of the difference concerns the X-ray domain, which lies above ν_c . The spectrum is computed as follows.

At frequencies $< \nu_c$, the standard synchrotron spectrum holds, although the magnetic field value should be taken as the partially decayed micro-turbulent value at the back of the blast, which evolves in time:

$$\delta B_- \simeq \delta B_+ (t_{\text{dyn}}/\tau_{\delta B})^{\alpha_t/2} \propto \epsilon_{B+}^{1/2} t_{\text{obs}}^{(\alpha_t-6)/8}. \quad (28)$$

Of course, one recovers the standard time evolution in the limit $\alpha_t \rightarrow 0$.

At frequencies $\nu_c < \nu < \hat{\nu}_c$, i.e. if $\nu_c < \hat{\nu}_c$ ($\hat{\nu}_c$ designating the synchrotron peak frequency associated with $\hat{\gamma}_c$), KN suppression is ineffective, $\Upsilon_{\text{KN}}(\nu) < 1$; therefore, the electrons cool in a uniform radiation background, but radiate their synchrotron flux in a changing magnetic field, all along their cooling history. This leads to a synchrotron spectral index

$$\beta = \frac{p + \alpha_t/2}{2 - \alpha_t/2} \quad [\nu > \nu_c, \Upsilon_{\text{KN}}(\nu) < 1], \quad (29)$$

see the Appendix of Lemoine (2013), section A3.

To account for the influence of KN suppressed inverse Compton losses at frequencies $\nu > \max(\nu_c, \hat{\nu}_c)$, we proceed as follows. We first solve for γ_c and Y_c as in equations 3 and 4, using however a value δB_- for the magnetic field at the back of the blast. We then solve for the cooling history $\gamma_e(t)$ of an electron with initial Lorentz factor (meaning at the shock front, t representing the co-moving since acceleration at the shock) $\gamma_{e,0} > \gamma_c$, considering that if $\Upsilon_{\text{KN}}(\nu) > 1$, this electron interacts with a radiation field of energy density $Y(\gamma_e)\delta B_-^2/(8\pi)$, characterized by the Lorentz factor dependent Compton parameter $Y(\gamma_e)$ (e.g. Li & Waxman 2006; Nakar et al. 2009; Wang et al. 2010):

$$Y(\gamma_e) \simeq Y_c \left(\frac{\gamma_e}{\gamma_c} \right)^{(p-3)/2}, \quad (30)$$

assuming $\hat{\gamma}_c < \gamma_c < \gamma_e$. Here as well, we can neglect extreme cases in which the electron interacts with the low-frequency bands of the spectrum, below ν_{min} . Solving for the cooling history in this radiation field, one determines a cooling time-scale $t_{\text{cool}}(\gamma_{e,0}) \simeq t_{\text{dyn}}(\gamma_{e,0}/\gamma_c)^{-2/(p-1)/2}$, and $\gamma_e(t) \simeq \gamma_c(t/t_{\text{dyn}})^{-2/(p-1)}$

for $t \gg t_{\text{cool}}(\gamma_{e,0})$. Following Lemoine (2013), we then calculate the individual electron synchrotron contribution, by integrating the synchrotron power $\propto \gamma_e^2(t)\delta B^2(t)$ over this cooling history; then we evaluate the contribution of the electron population by folding the latter result over the injection distribution function of electron Lorentz factors. This leads to a synchrotron spectral index

$$\beta = \frac{3(p-1)}{4} \frac{1 + \alpha_t/6}{1 - \alpha_t(p-1)/8} \quad [\nu > \nu_c, \Upsilon_{\text{KN}}(\nu) > 1], \quad (31)$$

which tends to $3(p-1)/4$ as it should when $\alpha_t \rightarrow 0$ (non-decaying turbulence).

Finally, at > 100 MeV, we assume that inverse Compton losses are negligible; hence, we use the above $\beta = (p + \alpha_t/2)/(2 - \alpha_t/2)$. This slight change of slope, as compared to the two-zone determinations, implies slightly different parameter values. The final estimates are given in the captions of Figs 1–4, which present the models of these multi-wavelength light curves.

We have not attempted to obtain least-squares fit to these multi-wavelength light curves, rather we have used the normalization of the flux at several data points, as discussed in the previous sections, derived the parameters, then plotted the predicted multi-wavelength light curves. We have also neglected the possibility of significant extinction in the optical domain, which could improve the quality of the fit for GRB 110731A in particular. Moreover, our numerical code computes the light curves for a decelerating blast wave; it does not account for the initial ballistic stage, and neither does it account for sideways expansion beyond jet break. We have chosen to plot the > 100 MeV light curve assuming deceleration of the blast beyond 10 s, which corresponds to initial Lorentz factors > 700 for GRB 110731A and GRB 090902B, for which > 100 MeV data exist at 10 s; one should note, however, that the deceleration regime becomes valid beyond T_{90} , which marks the duration of the prompt emission, and $T_{90} = 150, 70, 25$ and 8 s for GRB 090323, GRB 090328, GRB 090902B and GRB 110731A, respectively (Ackermann et al. 2013b). Evidence for jet break is

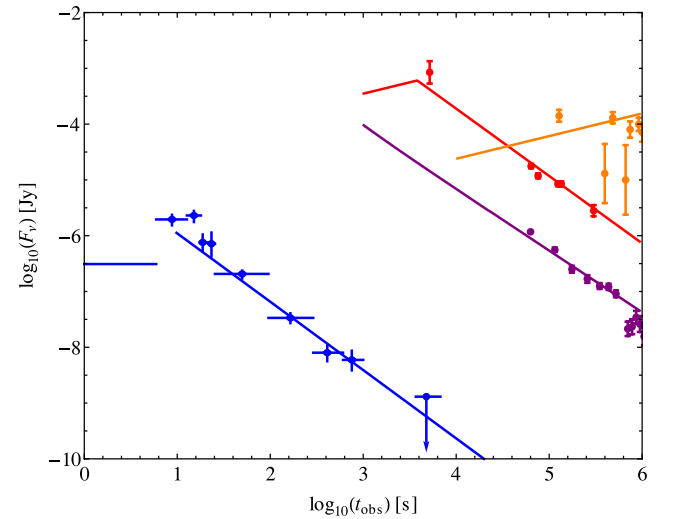


Figure 1. Multi-wavelength light curve for GRB 090902B; orange: radio flux density, red: optical R-band flux density, purple: X-ray flux $\int_{0.3 \text{ keV}/h}^{10 \text{ keV}/h} F_\nu d\nu / (2.4 \times 10^{17} \text{ Hz})$, blue: spectral flux density F_ν at $2.4 \times 10^{22} \text{ Hz}$; parameter values: $E = 1.6 \times 10^{54} \text{ erg}$, $n = 0.012 \text{ cm}^{-3}$, $\epsilon_e = 0.50$, $p = 2.3$, $k = 0$ and $\alpha_t = -0.45$. Data taken from Cenko et al. (2011) and Abdo et al. (2009) and the *Swift* XRT repository data base (Evans et al. 2007, 2009).

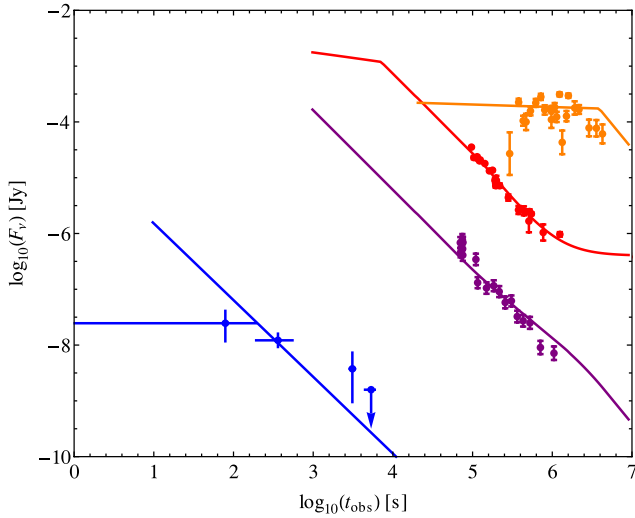


Figure 2. Same as Fig. 1, for GRB 090323, except that the blue data indicates the >100 MeV flux $\int_{100\text{MeV}/h} F_\nu d \ln \nu$. Parameter values: $E=5.4 \times 10^{54}$ erg, $A=8.4 \times 10^{35}$ cm $^{-1}$, $\epsilon_e=0.29$, $p=2.5$, $k=2$ and $\alpha_t=-0.54$. Data taken from Cenko et al. (2011), Piron, McEnery & Vasileiou (2011) and the *Swift* XRT repository data base (Evans et al. 2007, 2009); a constant R -band flux of 4×10^{-7} Jy models the host galaxy emission.

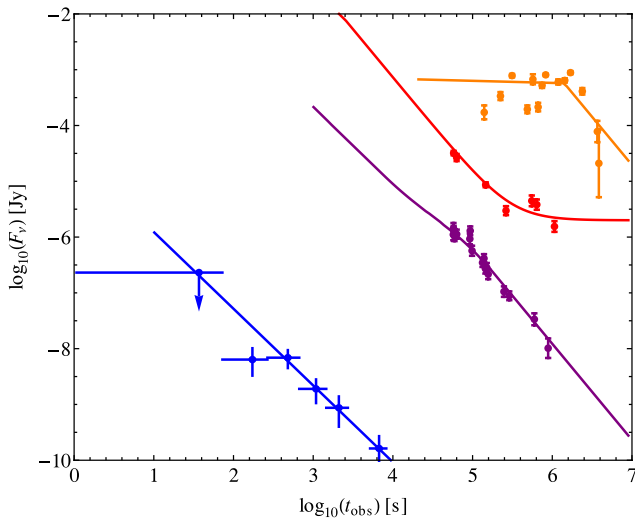


Figure 3. Same as Fig. 2, for GRB 090328 (using U -band optical data). Parameter values: $E=0.73 \times 10^{54}$ erg, $A=1.5 \times 10^{35}$ cm $^{-1}$, $\epsilon_e=0.18$, $p=2.5$, $k=2$ and $\alpha_t=-0.45$. Data taken from Cenko et al. (2011), Piron et al. (2011) and the *Swift* XRT repository data base (Evans et al. 2007, 2009); a constant R -band flux of 2×10^{-6} Jy models the host galaxy emission.

lacking in the four bursts, except possibly for GRB 090902B (Cenko et al. 2011), in which case it would improve the fit at times $\gtrsim 10^6$ s. Thus, there is room for improving the quality of these fits, but it should not modify the value of α_t derived in the previous sections beyond the quoted uncertainties.

Finally, using the solutions indicated in the captions of the figures, one can verify that synchrotron self-absorption effects are negligible in the radio domain at the time at which the flux was normalized to the data. One can also verify that for all bursts except GRB 090323, the inverse Compton component provides a negligible contribution at >100 MeV at early times; for GRB 090323, this

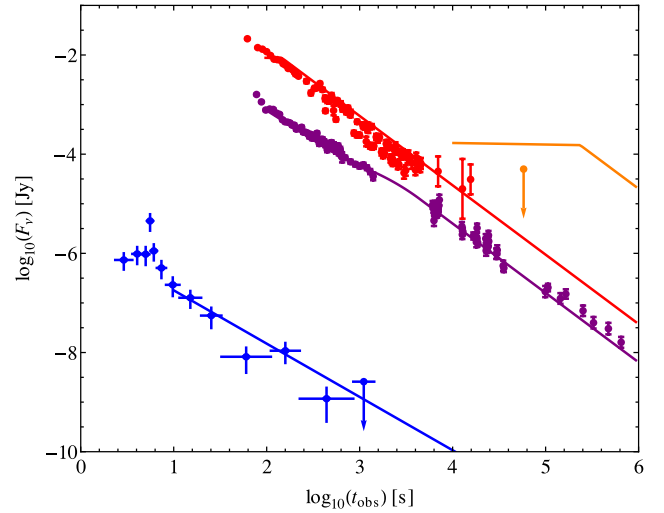


Figure 4. Same as Fig. 2, for GRB 110731A with in the optical range: UVOT v -band optical data, UVOT w -band data scaled to the v -band data, MoA I - and V -band data. Parameter values: $E=6.7 \times 10^{54}$ erg, $A=0.15 \times 10^{35}$ cm $^{-1}$, $\epsilon_e=0.035$, $p=2.1$, $k=2$ and $\alpha_t=-0.38$. Data taken from Ackermann et al. (2013a) and the *Swift* XRT repository data base (Evans et al. 2007, 2009).

contribution is a factor of 0.6 of the observed flux at $t_{\text{obs}}=360$ s, thus non negligible. However, this remains within the error bars on the flux normalization that we have adopted for this GRB; therefore, we neglect its influence. Future work should consider more detailed multi-wavelength light curves including this inverse Compton component, and possibly as well the effect of the maximal energy in the >100 MeV domain, as in Wang et al. (2013).

3 DISCUSSION

In the present work, we have argued that the afterglow of four GRBs observed in the radio, optical, X-ray and at >100 MeV by the *Fermi*-LAT instrument can be explained as synchrotron radiation in a decaying micro-turbulence; such micro-turbulence and its decay through collisionless phase mixing are expected on theoretical grounds, as consequences of the formation of a relativistic collisionless shock in a weakly magnetized environment. We have modelled the multi-wavelength light curves of these four GRBs using first a simplified two-zone model for the decaying turbulence, characterized in particular by ϵ_{B-} , which represents the value of ϵ_B at the rear of the blast, where radio, optical and X-ray photons are produced, and $\epsilon_{B+} \sim 0.01$, close to the shock where the micro-turbulence has not yet had time to relax. Then we have used a full synchrotron calculation assuming a power-law-decaying micro-turbulence to improve on the above simplified model.

The low values of ϵ_{B-} that we derive here agree well with those derived by Kumar & Barniol-Duran (2009, 2010), Barniol-Duran & Kumar (2011), He et al. (2011) and Liu & Wang (2011). There are however important differences in the interpretation of these low values: Kumar & Barniol-Duran (2009, 2010) argue that all particles cool in the background shock compressed magnetic field (including those producing >100 MeV photons), which is inferred of the order of $\sim 10 \mu\text{G}$ (upstream rest frame). We rather argue that the particles cool in the post-shock decaying micro-turbulence, which is self-generated in the shock precursor through micro-instabilities and which actually builds up the collisionless shock. As discussed in the introduction, this latter interpretation

is motivated by the large hierarchy between the inferred values of $\epsilon_{B-} \sim 10^{-6}$ to 10^{-4} and the much smaller interstellar magnetization level $\sim 10^{-9}$, indicating that the background shock compressed field plays no role in shaping the light curves. A power-law decay of the micro-turbulence behind the shock front is also theoretically expected, e.g. Chang et al. (2008). Furthermore, we provide a complete self-consistent model of the synchrotron afterglow light curves in this scenario, based on and improving the results of Lemoine (2013). Within our interpretation, we are thus able to constrain the value of the exponent of the decaying micro-turbulence (assuming power-law decay), and we find a consistent value among all bursts studied, $-0.5 \lesssim \alpha_t \lesssim -0.4$. This value turns out to agree quite well with the results of the PIC simulations of Keshet et al. (2009), see the discussion in Lemoine (2013).

These low values of ϵ_{B-} stand in stark contrast with other determinations by Cenko et al. (2011) for GRB 090902B, GRB 090323 and GRB 090328, and by Ackermann et al. (2013a) for GRB 110731A, who systematically find values $\epsilon_B \sim 0.01$. The key difference turns out to come from the high-energy component > 100 MeV. While in the present work, we assume that this extended emission is synchrotron radiation from shock-accelerated electrons, those studies do not incorporate the constraints from the high-energy component. Using the best-fitting models of Cenko et al. (2011) and Ackermann et al. (2013a), it is straightforward to calculate the ratio $R_{>100\text{MeV}}$ of the predicted photon flux $\phi(>100\text{MeV})$ to the observed values:³

$$\begin{aligned} 090902\text{B} : R_{>100\text{MeV}} &\simeq 7.2 \times 10^{-2} \quad (t_{\text{obs}} = 50 \text{ s}) \\ 090323 : R_{>100\text{MeV}} &\simeq 3.5 \times 10^{-3} \quad (t_{\text{obs}} = 350 \text{ s}) \\ 090328 : R_{>100\text{MeV}} &\simeq 1.9 \times 10^{-2} \quad (t_{\text{obs}} = 1100 \text{ s}) \\ 110731\text{A} : R_{>100\text{MeV}} &\simeq 1.1 \times 10^{-2} \quad (t_{\text{obs}} = 30 \text{ s}) . \end{aligned} \quad (32)$$

The result is rather striking: those models do not explain the high-energy component, in spite of the excellent quality of the fits obtained in the other domains, e.g. Cenko et al. (2011). Ultimately, this results from degeneracy in the parameter space, when only three wavelength bands are used to determine the four parameters E , n , ϵ_e and ϵ_B (assuming that some extra information is available to determine p and k , e.g. the time behaviour). Specifically, the models of Cenko et al. (2011) and Ackermann et al. (2013a) present solutions that are degenerate up to the choice of one of the above parameters, say ϵ_e . To verify this, one can explicitly repeat the above exercises, neglecting the >100 MeV data. By tuning ϵ_e , one can then find similar light curves, with different values of the parameters. These different sets of solutions also correspond to different values of Y_c ; the solutions of Cenko et al. (2011) and Ackermann et al. (2013a) systematically have $Y_c \lesssim 1$, while ours rather corresponds to $Y_c \gg 1$. When $Y_c > 1$, the solution scales differently with ϵ_e , because of the influence of inverse Compton losses in the X-ray domain (notwithstanding possible KN suppression). As $Y_c \gg 1$, one recovers our solutions up to the ambiguity in the choice of ϵ_e . This ambiguity is eventually raised by the normalization to the >100 MeV flux, leading to the present low ϵ_B values.

Going one step further, one should envisage the possibility that earlier (pre-*Fermi*) determinations of the microphysical parameters could be affected by a similar bias. The detailed analysis of Panaitescu & Kumar (2001, 2002) indicates indeed a broad range of values of ϵ_{B-} for any GRB, spanning values from $\sim 10^{-6}$ up to

10^{-1} . Thus, ϵ_{B-} is poorly known. In very few cases, such as the famous GRB 970508, a synchrotron self-absorption break seems to appear in the radio band. In these cases, using the radio data in both optically thin and thick regimes, as well as the optical and X-ray data, one has four bands for four parameters, then all the parameters can be determined. A large value for the magnetic field, $\epsilon_{B-} \sim 0.01$, is obtained for GRB 970508 by Wijers & Galama (1999). However, the absorption break in radio may not be clear given the bad quality of radio data (due to strong scintillation). A recent re-analysis of GRB 970508 by Leventis et al. (2013) also finds a variety of solutions, including one with a low value of ϵ_{B-} , when no ad hoc extra constraint is imposed on the parameters. Future work should consider carefully the uncertainty in the determination of ϵ_{B-} in such bursts.

Taken at face value, the present results suggest that the magnetization of the blast can be described as the partial decay of the micro-turbulence that is self-generated at the shock; it also suggests that evidence for further amplification of this turbulence is lacking, at least in the bursts observed by the *Fermi*-LAT instrument.

While this paper was being completed, GRB 130427A has been observed with the *Fermi*-LAT instrument with unprecedented statistics, with detailed follow-up observations in the radio, optical and X-ray (see e.g. Laskar et al. 2013; Fan et al. 2013; Tam et al. 2013, and references therein). As discussed in Tam et al. (2013), this GRB presents strong evidence for the emergence of the SSC component at high energies $\gtrsim 1$ – 10 GeV above the synchrotron component. In a forthcoming paper, Liu, Wang & Wu (2013) model the multi-wavelength light curve of this GRB in a similar spirit to the present analysis and derive in particular a value $\epsilon_B = 1.7 \times 10^{-5}$. From their afterglow parameters, one then infers $\alpha_t \simeq -0.44$, in excellent agreement with the values derived here.

ACKNOWLEDGEMENTS

We thank F. Piron for useful discussions. This work has been supported in part by the PEPS/PTI programme of the INP (CNRS), by the NSFC (11273005), the MOE PhD Programmes Foundation, China (20120001110064) and the CAS Open Research Programme of Key Laboratory for the Structure and Evolution of Celestial Objects, as well as the 973 Programme under grant 2009CB824800, the NSFC under grants 11273016, 10973008 and 11033002, the Excellent Youth Foundation of Jiangsu Province (BK2012011). This work made use of data supplied by the UK Swift Science Data Centre at the University of Leicester.

REFERENCES

- Abdo A. A. et al. (Fermi Collaboration), 2009, *ApJ*, 706, L138
 Ackermann et al. (Fermi Collaboration), 2013a, *ApJ*, 763, 71
 Ackermann et al. (Fermi Collaboration), 2013b, preprint (arXiv:1303.2908)
 Barniol-Duran R., Kumar P., 2011, *MNRAS*, 417, 1584
 Bykov A., Gehrels N., Krawczynski H., Lemoine M., Pelletier G., Pohl M., 2012, *Space Sci. Rev.*, 173, 309
 Cenko S. B. et al., 2011, *ApJ*, 732, 29
 Chang P., Spitkovsky A., Arons J., 2008, *ApJ*, 674, 378
 Evans P. A. et al. (Swift-XRT), 2007, *A&A*, 469, 379
 Evans P. A. et al. (Swift-XRT), 2009, *MNRAS*, 397, 1177
 Fan Y.-Z. et al., 2013, preprint (arXiv:1305.1261)
 Gruzinov A., Waxman E., 1999, *ApJ*, 511, 852
 Haugbølle T., 2011, *ApJ*, 739, 42
 He H.-N., Wu X.-F., Toma K., Wang X.-Y., Mészáros P., 2011, *ApJ*, 733, 22
 Keshet U., Katz B., Spitkovsky A., Waxman E., 2009, *ApJ*, 693, L127
 Kirk J., Reville B., 2010, *ApJ*, 710, 16

³ For GRB 090902B, we rather compare the spectral flux density at 2.4×10^{22} Hz to the observed value.

- Kumar P., Barniol-Duran R., 2009, MNRAS, 400, L75
Kumar P., Barniol-Duran R., 2010, MNRAS, 409, 226
Laskar T. et al., 2013, preprint (arXiv:1305.2453)
Lemoine M., 2013, MNRAS, 428, 845
Lemoine M., Pelletier G., Revenu B., 2006, ApJ, 645, L129
Leventis K., van der Horst A. J., van Eerten H. J., Wijers R. A. M. J., 2013, MNRAS, 431, 1026
Li Z., Waxman E., 2006, ApJ, 651, L328
Liu R., Wang X.-Y., 2011, ApJ, 730, 1
Liu R., Wang X.-Y., Wu X.-F., 2013, ApJ, 773, L20
Lyutikov M., 2010, MNRAS, 405, 1809
Martins S. F., Fonseca R. A., Silva L. O., Mori W. B., 2009, ApJ, 695, L189
Medvedev M. V., Loeb A., 1999, ApJ, 526, 697
Medvedev M. V., Trier Frederiksen J., Haugboelle T., Nordlund A., 2011, ApJ, 737, 55
Nakar E., Ando S., Sari R., 2009, ApJ, 703, 675
Panaitescu A., Kumar P., 2001, ApJ, 554, 667
Panaitescu A., Kumar P., 2002, ApJ, 571, 779
Piran T., 2004, Rev. Mod. Phys., 76, 1143
Piron F., McEnery J., Vasileiou V., 2011, AIP Conf. Ser. Vol. 1358, Gamma Ray Bursts 2010. Am. Inst. Phys., New York, p. 47
Plotnikov I., Pelletier G., Lemoine M., 2013, MNRAS, 430, 1208
Sari R., Esin A. A., 2001, ApJ, 548, 787
Sari R., Piran T., Narayan R., 1998, ApJ, 497, L17
Sironi L., Spitkovsky A., 2011, ApJ, 726, 75
Sironi L., Spitkovsky A., 2013, ApJ, 771, 54
Spitkovsky A., 2008, ApJ, 682, L5
Tam P.-H. T., Tang Q.-W., Hou S., Liu R.-Y., Wang X.-Y., 2013, ApJ, 771, L13
Wang X.-Y., He H.-N., Li Z., Wu X.-F., Dai X.-G., 2010, ApJ, 712, 1232
Wang X.-Y., Liu R., Lemoine M., 2013, ApJ, 771, L33
Wijers R. A. M. J., Galama T. J., 1999, ApJ, 523, 177
Zauderer A., Berger E., Frail D. A., 2011, GRB Coordinates Network, Circular Service, 12227, 1

This paper has been typeset from a $\text{\TeX}/\text{\LaTeX}$ file prepared by the author.